Journal of Nuclear Materials 401 (2010) 138–142

Contents lists available at ScienceDirect

Journal of Nuclear Materials

journal homepage: www.elsevier.com/locate/jnucmat

Local and electronic structure of Am_2O_3 and AmO_2 with XAFS spectroscopy

Tsuyoshi Nishi [a,*], Masami Nakada [a], Chikashi Suzuki [a], Hiroki Shibata [a], Akinori Itoh [a], Mitsuo Akabori [a], Masaru Hirata [b]

[a] Nuclear Science and Engineering Directorate, Japan Atomic Energy Agency, Tokai-mura, Ibaraki 319-1195, Japan
[b] Advanced Nuclear System Research and Development Directorate, Japan Atomic Energy Agency, Oarai-machi, Ibaraki 311-1393, Japan

ARTICLE INFO

Article history:
Received 9 July 2009
Accepted 14 April 2010

ABSTRACT

XAFS studies were performed in a study of americium sesquioxide (Am_2O_3) with A-type rare earth oxide structure and americium dioxide (AmO_2) with fluorite structure. EXAFS results on the Am-L_{III} absorption edge of Am_2O_3 and AmO_2 were in good agreement with crystallographic data resulting from X-ray diffraction analysis. Theoretical assignments were performed using the all-electron Full Potential Linearized Augmented Plane Wave (FP-LAPW) method in characterizing XANES with regard to the electronic structure of Am_2O_3 and AmO_2. The theoretical XANES spectra of Am_2O_3 and AmO_2 well reproduced the experimental ones. In addition, it was found that the white line peak was created due to the interaction between the Am-d and O-p components, and the broad peak and the tail peak were created due to the interaction between the Am-d and O-d components.

1. Introduction

Minor Actinides (MAs) accumulate in irradiated nuclear fuel. Among MAs, americium (Am) has high and lasting radiotoxicity. In addition, the oxidation state of Am ions varies at high temperatures due to their high oxygen potential. Many types of advanced Am containing fuels, including Am mixed oxide (Am–MOX) fuels, have been investigated for use in Fast Reactors (FRs), they include the problem of resulting in oxidation of the cladding tubes by the excess oxygen generating because of the reduction from Am^{4+} at high temperatures. For this reason, identifying the local and electronic structure around Am atom in Am oxide is indispensable information on advanced Am containing fuels.

The X-ray Absorption Fine Structure (XAFS) technique that includes the Extended X-ray Absorption Fine Structure (EXAFS) and the X-ray Absorption Near-Edge Structure (XANES) techniques is an excellent method of examining the local and electronic structure surrounding actinide atoms in oxide fuels [1–5]. In particular, XANES is very useful in determining the symmetry, bond distance, and electronic structure around the absorbing atom.

Martin and co-workers utilized the XAFS technique in investigating the local structure of actinide atoms and simulated fission products in UO_2 and other oxide fuels [3–5]. They demonstrated the efficacy of EXAFS in studying the local structure of these minor constituents of fuel matrixes. Recently, XAFS studies on Am containing oxides: (Zr, Y, Am)O_{2-x} [6] and $Am_2Zr_2O_7$ [7] have also taken place. However, despite the importance of the structural and electronic information on pure Am oxides, XAFS studies on pure Am oxides have been scarce due to experimental difficulties.

In this paper, the XAFS measurements at Am-L_{III} absorption edge of Am_2O_3 and AmO_2 were performed in transmission mode. The EXAFS spectrum was then analyzed in the conventional way using a computer program in proving the validity of the experimental EXAFS and XANES spectra. Moreover, the theoretical assignment of the Am-L_{III} XANES spectra of Am_2O_3 and AmO_2 took place using the all-electron FP-LAPW method in investigating the electronic structure as a fundamental evaluation tool with Am oxides.

2. Experimental

2.1. Am_2O_3 sample preparation

Stoichiometric Am_2O_3 powder for use in the XAFS measurements was prepared by heating $^{243}AmO_2$ powder at 1273 K for 2 h in N_2 + 4% H_2 mixture gas flow. The purity of the AmO_2 powder was about 99.7% with regard to nonradioactive impurities [8]. The sample was also examined by powder X-ray diffraction analysis with Cu Kα radiation to identify the phases and to determine the lattice parameter. The X-ray diffraction pattern is shown in Fig. 1, where ZrN powder was used as an internal standard. The X-ray diffraction analysis revealed the sample to be composed of a hexagonal phase with lattice parameters of 0.3818 nm for the *a*-axis and 0.5980 nm for the *c*-axis. The lattice parameters esti-

* Corresponding author. Address: Research Group for Transuranium Fuels Behavior and Properties, Division of Fuels and Materials Engineering, Nuclear Science and Engineering Directorate, Japan Atomic Energy Agency, Shirakata-Shirane 2-4, Tokai-mura, Ibaraki-ken 319-1195, Japan. Tel.: +81 29 282 5431; fax: +81 29 282 6122.
E-mail address: nishi.tsuyoshi@jaea.go.jp (T. Nishi).

0022-3115/$ - see front matter © 2010 Elsevier B.V. All rights reserved.
doi:10.1016/j.jnucmat.2010.04.011

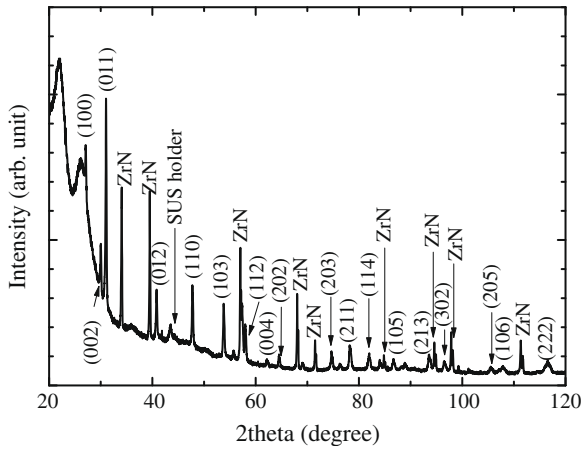

Fig. 1. X-ray diffraction pattern of Am_2O_3 (hexagonal phase) together with ZrN powder as an internal standard.

mated using the X-ray diffraction pattern were almost the same as values found in literature (0.38155 nm for the *a*-axis and 0.5975 nm for the *c*-axis) [9].

The Am_2O_3 and graphite powder was stirred and pressed into a disk of 6 mm in diameter. The Am_2O_3 weighed 5.5 mg, corresponding to 37 MBq, while the graphite weighed 37.5 mg. The optimum sample thickness of Am_2O_3 in the transmission XAFS measurements was determined using the equation $\Delta\mu t = 1$, where $\Delta\mu$ is the absorption edge jump of Am and t the optimum sample thickness. The optimum sample thickness estimated using the $\Delta\mu$ of Am [10] was identified in the calculations to be 13.5 μm. The disk was doubly sealed in two polyethylene terephthalate (PET) containers using epoxy resin (stycast 1266).

2.2. XAFS measurements

XAFS measurements at the Am-L_{III} absorption edge of Am_2O_3 took place in transmission mode at the hard X-ray station BL-27 in the Photon Factory of High Energy Accelerator Research Organization (KEK) at an energy level of 2.5 GeV. The radiation was monochromatized using a double-crystal Si(1 1 1) monochromator. The intensity of the incident and transmitted beams was monitored utilizing an ionization chamber with a flow of Ar/N_2 gas and Ar gas, respectively. EXAFS and XANES spectra were both recorded at room temperature. Energy calibration of EXAFS and XANES spectra were achieved using the Zr foil (K-edge: 17.998 keV [11]) references positioned in front of the sample. XAFS measurements at the Am-L_{III} edge of AmO_2 had already been performed. The detailed information was described in Ref. [12].

The EXAFS spectrum was analyzed in the conventional way with the computer program WinXAS (version 3.1) [13] in proving the validity of the experimental EXAFS and XANES spectra. The atomic distances and coordination numbers were determined through fitting the inverse Fourier transformation of the isolated contribution of the interest shells on the R-space distributions to the EXAFS equation, where the EXAFS analysis was based on the back-scattering amplitudes and phase shifts calculated in FEFF 8 (version 8.4) code [14] theoretical calculations using the crystallographic data resulting from XRD analysis.

2.3. XANES analyses

The XANES spectra were analyzed using the all-electron FP-LAPW method, as implemented using Wien2k code [15] within the framework of Density Functional Theory (DFT). In the calculations, relativistic effects were fully introduced for the core-electrons by solving the Dirac equation, while the valence electrons were treated within the scalar relativistic approximation. The exchange–correlation energy was described within the Generalized Gradient Approximation (GGA) [16] with a Hubbard U parameter, which applied to Am-d orbitals is 7.0 eV. The muffin-tin radii of Am and O were set to be 2.26 and 2.10 bohr, respectively. The cut-off parameter $R_{MT}K_{max}$ used to limit the number of plane waves was set to be 7.0, where R_{MT} is the smallest value of all the atomic sphere radii and K_{max} the largest reciprocal lattice vector used in the plane wave expansion. In order to avoid any interactions between adjacent core–holes, calculations were performed on a $3 \times 3 \times 2$ supercell (90 atoms) for Am_2O_3 and a $2 \times 2 \times 2$ supercell (96 atoms) for AmO_2. In addition, a *k*-point sampling mesh of $3 \times 3 \times 3$ for the reciprocal space of the supercell for both Am_2O_3 and AmO_2 was used. The theoretical spectra were calculated within the electronic-dipole-allowed transition in the core–hole state. The core–hole effects were fully taken into account in the calculations by removing one electron from the Am $2p_{3/2}$ orbital of interest and putting one additional electron to the bottom of the conduction band. The theoretical spectra were convoluted with a Gaussian function of 12.0 eV Full Widths at Half Maximum (FWHM). The unoccupied Partial Densities Of States (PDOS) were convoluted with the Gaussian function of 0.5 eV FWHM.

3. Results and discussion

3.1. Verifications of Am_2O_3 and AmO_2 EXAFS and XANES spectra

Fig. 2 shows the EXAFS and XANES spectra of the Am-L_{III} absorption edge of Am_2O_3 and AmO_2. Two peaks (peaks A, B) and tail peak A′ can be observed in XANES spectra. An energy shift of a white line

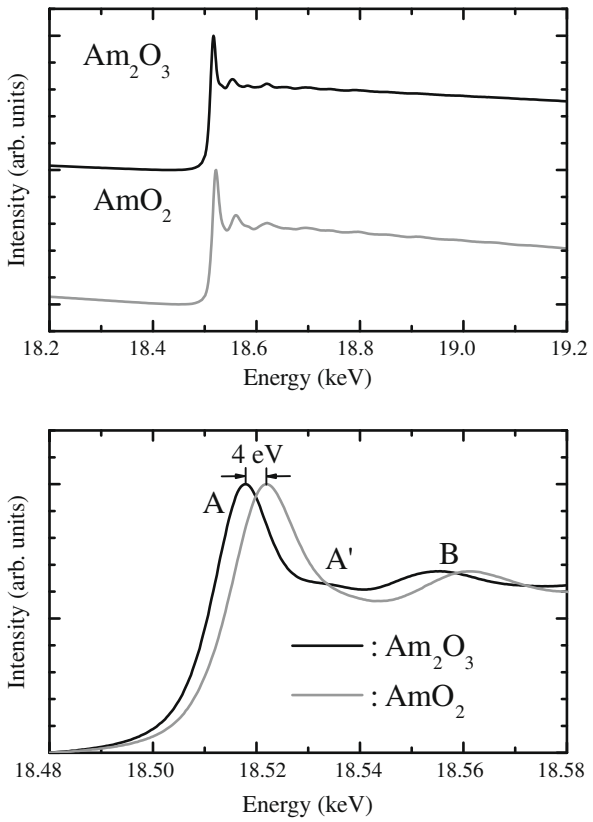

Fig. 2. Experimental EXAFS and XANES spectra of Am-L_{III} absorption edge of Am_2O_3 and AmO_2 [12].

peak was also observed at about 4 eV, which is consistent with the chemical shift between Am^{3+} and Am^{4+}. EXAFS analysis was performed in view of the effect of the main multiple scattering using the atomic distances and coordination numbers of Am_2O_3 and AmO_2 that were calculated with crystallographic data obtained from X-ray diffraction analysis (refer to Table 1). The resultants k^3-weighted EXAFS oscillations of Am_2O_3 and AmO_2 [12] are provided in Fig. 3, where the broken line corresponds to the calculated data in fitting it to the experimental data. The obtained EXAFS oscillations of Am_2O_3 and AmO_2 covered the wave vector of k up to 150 nm^{-1} and 170 nm^{-1}, which proved wide enough to obtain a sufficiently resolved Fourier transformation of the EXAFS oscilla-

Table 1
Atomic distances and coordination numbers of (a) AmO_2 and (b) Am_2O_3 calculated using crystallographic data resulting from X-ray diffraction analysis.

Shell	Distance (nm)	Coord. no.
(a)		
Am–O	0.2329	8
Am–Am	0.3804	12
Am–O	0.4460	24
(b)		
Am–O	0.2299	3
Am–O	0.2386	1
Am–O	0.2650	3
Am–O	0.3594	1
Am–Am	0.3676	3
Am–Am	0.3753	3
Am–Am	0.3818	6
Am–O	0.4457	3
Am–O	0.4502	6
Am–O	0.4648	3

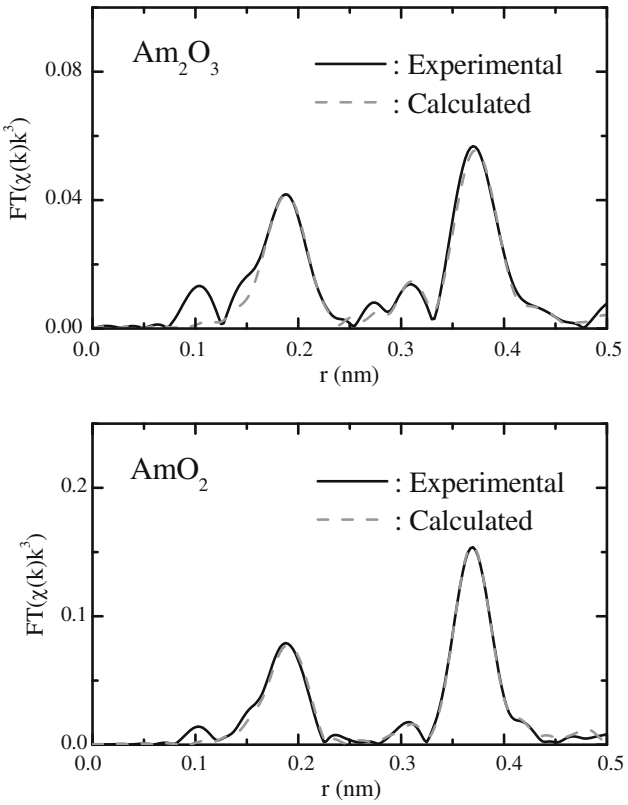

Fig. 4. R-space distributions of Am-L_{III} absorption edge of Am_2O_3 and AmO_2.

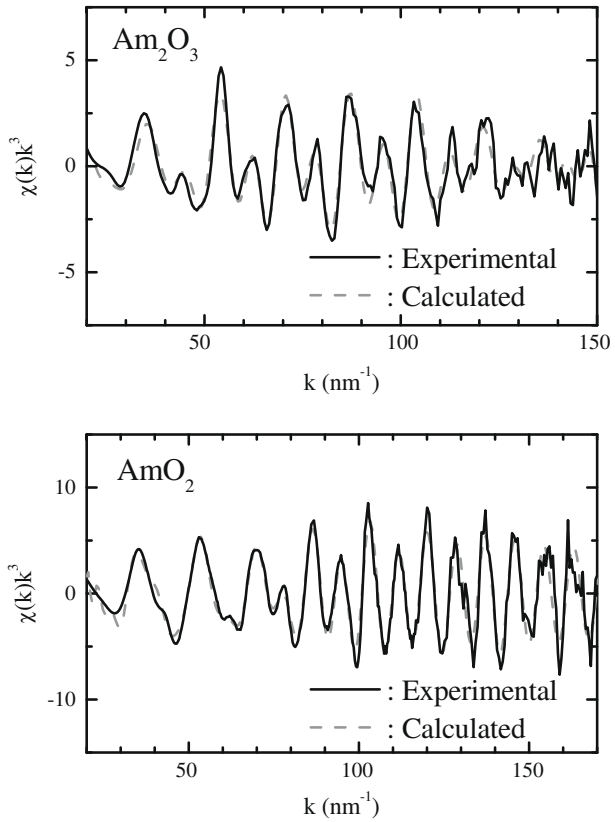

Fig. 3. k^3-Weighted EXAFS oscillations of Am-L_{III} absorption edge of Am_2O_3 and AmO_2.

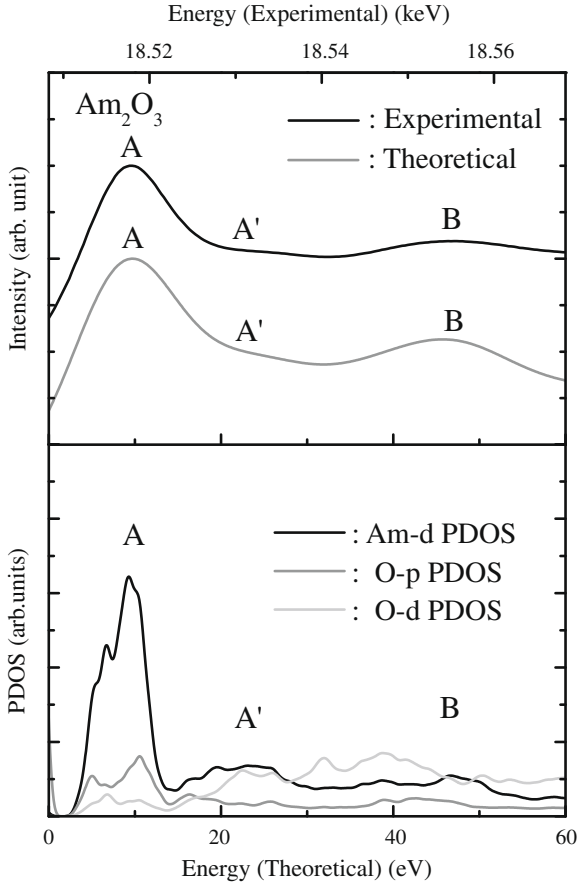

Fig. 5. Experimental and theoretical XANES spectra of Am_2O_3 together with the PDOS of Am-d, O-p and O-d atoms.

tion. As shown in Fig. 3, it was found that good agreement between experimental EXAFS oscillations and calculated one. In addition, the Fourier transformation of the EXAFS oscillation is shown in Fig. 4. It was also found that good agreements between experimental Fourier transform of EXAFS oscillation and calculated one. Thus, it can be concluded that the experimental Am-L_{III} EXAFS and XANES spectra of Am_2O_3 and AmO_2 are high-quality spectra that can be used to obtain useful information on local and electronic structure.

3.2. Electronic structure of Am_2O_3 and AmO_2 related with XANES spectra

The experimental and theoretical XANES spectra of the Am-L_{III} absorption edge and the major components of PDOS, Am-d, O-p and O-d of Am_2O_3 and AmO_2 are shown in Figs. 5 and 6. The energy of the Highest Occupied Molecular Orbital (HOMO) was set to be zero for the theoretical XANES spectra. The experimental and theoretical spectra aligned in the peak A position. It was found that the both the experimental XANES spectra could be considered to be basically the same, although the tail peak A′ of Am_2O_3 was slightly larger than that of AmO_2. The different tail structure may have been caused by the structure of the adjacent O atoms around Am. The theoretical XANES spectra of both Am_2O_3 and AmO_2 well reproduced the experimental ones regardless of the difference of symmetry. It was also found that the XANES spectrum of the Am-L_{III} absorption edge was mainly constructed from Am-d component in Am_2O_3 and AmO_2. With respect to the contribution of the O component in Am_2O_3 and AmO_2, the O-p component was dominant at peak A, while the O-d component was dominant in the higher energy range around peak B and tail peak A′. Therefore, the peak A was created due to the interaction between the Am-d and O-p components, while the peak B and the tail peak A′ resulted from the interaction of the Am-d and O-d components.

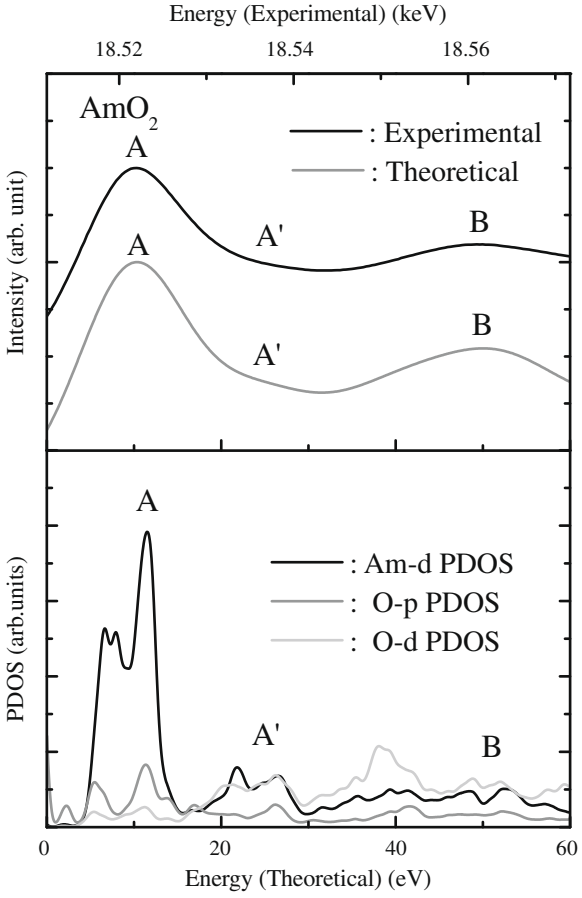

Fig. 6. Experimental and theoretical XANES spectra of AmO_2 together with the PDOS of Am-d, O-p and O-d atoms.

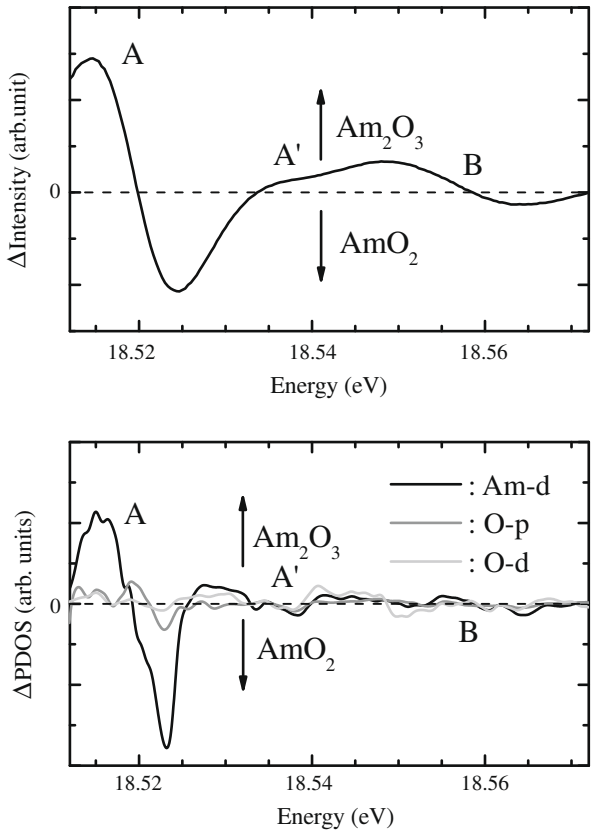

Fig. 7. Differential XANES spectrum and differential PDOS. The differential data was calculated by subtracting that of AmO_2 from that of Am_2O_3.

Differential XANES spectrum and differential PDOS were obtained in order to investigate the relationship between the XANES spectra and the electronic structure. The differential ones were calculated by subtracting those of AmO_2 from those of Am_2O_3. The differential XANES spectrum and the differential PDOS are also plotted in Fig. 7. From these results, the XANES spectrum of the Am-L_{III} absorption edge was mainly constructed from the Am-d component in Am_2O_3 and AmO_2. In the range of the peak A, the O-p component was stronger than the O-d component. On the other hand, in the range of the peak B and the tail peak A′, O-d component was slightly stronger than the O-p component. Accordingly, in the range of the white line peak, the interaction between the Am-d and O-p components was stronger than that between the Am-d and O-d components, and then, in the range of the broad peak and the tail peak, the interaction between the Am-d and O-d components was slightly stronger than that between the Am-d and O-p components.

4. Conclusions

The EXAFS and XANES spectra of Am_2O_3 were successfully obtained through transmission XAFS measurements. XANES analysis was then utilized to explain the different electronic structure around Am atoms in Am_2O_3 and AmO_2. The conclusions were as follows:

(1) The EXAFS results of Am_2O_3 and AmO_2 were in good agreement with the crystallographic data resulting from X-ray diffraction analysis. Therefore, the experimental Am-L_{III} EXAFS and XANES spectra of Am_2O_3 and AmO_2 can be considered as high-quality spectra for use in obtaining useful information on local and electric structure.
(2) The XANES spectra were analyzed using the all-electron FP-LAPW method implemented with Wien2k code and within the framework of DFT. The theoretical XANES spectra of both Am_2O_3 and AmO_2 well reproduced the experimental ones regardless of the difference of symmetry.
(3) In comparison with the electronic structure of Am_2O_3 and AmO_2, the interaction between the Am-d and O-p components was stronger than that between the Am-d and O-d components in the range of the white line peak and the interaction between the Am-d and O-d components was slightly stronger than that between the Am-d and O-p components in the range of the broad peak and the tail peak.

Acknowledgements

The authors would like to express their grateful to Prof. K. Kobayashi, the Institute of Materials Structure Science of High Energy Accelerator Research Organization (KEK), Drs. Y. Okamoto, A. Nakamura, Y. Kaji, Y. Arai and K. Minato, JAEA for their helpful advice, and Mr. M. Kamoshida, Chiyoda Maintenance Corporation for his kind supports.

References

[1] M.A. Denecke, Coord. Chem. Rev. 250 (2006) 730.
[2] K.E. Roberts, T.J. Wolery, C.E. Atkins-Duffin, T.G. Prussin, P.G. Allen, J.J. Bucher, D.K. Shuh, R.J. Finch, S.G. Prussin, Radiochim. Acta 91 (2003) 87.
[3] P. Martin, S. Grandjean, M. Ripert, M. Freyss, P. Blanc, T. Petit, J. Nucl. Mater. 320 (2003) 138.
[4] P. Martin, S. Grandjean, C. Valot, G. Carlot, M. Ripert, P. Blanc, C. Hennig, J. Alloys. Comp. 444–445 (2007) 410.
[5] P. Martin, M. Ripert, G. Carlot, P. Parent, C. Laffon, J. Nucl. Mater. 326 (2003) 132.
[6] M. Walter, C. Nästren, J. Somers, R. Jardin, M.A. Denecke, B. Brendebach, J. Solid State Chem. 180 (2007) 3130.
[7] P.M. Martin, R.C. Belin, P.J. Valenza, A.C. Scheinost, J. Nucl. Mater. 385 (2009) 126.
[8] T. Nishi, M. Takano, A. Itoh, M. Akabori, K. Minato, M. Kizaki, J. Nucl. Mater. 355 (2006) 114.
[9] C. Hurtgen, J. Fuger, Inorg. Nucl. Chem. Lett. 13 (1977) 179.
[10] Y. Waseda, Anomalous X-ray Scattering for Materials Characterization, Springer, Germany, 2002. pp. 205–207.
[11] J.A. Bearden, A.F. Burr, Rev. Mod. Phys. 39 (1967) 125.
[12] T. Nishi, M. Nakada, A. Itoh, C. Suzuki, M. Hirata, M. Akabori, J. Nucl. Mater. 374 (2008) 339.
[13] T. Ressler, J. Synchrotron. Radiat. 5 (1998) 118.
[14] A.L. Ankudinov, A.I. Nesvizhskii, J.J. Rehr, Phys. Rev. B 67 (2003) 115120.
[15] P. Blaha, K. Schwarz, G. Madsen, D. Kvascka, J. Luitz, WIEN2k, An Aurgmented Plane Wave + Local Orbital Program for Calculating Crystal Properties, Technische Universität Wien, Vienna, 2001.
[16] J.P. Perdew, K. Burke, M. Emzerhof, Phys. Rev. Lett. 77 (1996) 3865.